A SHORT NOTE ON MARINE RESERVOIR AGE SIMULATIONS USED IN INTCAL20

Martin Butzin[1]* • Timothy J Heaton[2] • Peter Köhler[1] • Gerrit Lohmann[1]

[1]Alfred-Wegener-Institut Helmholtz-Zentrum für Polar- und Meeresforschung, D-27515 Bremerhaven, Germany
[2]School of Mathematics and Statistics, University of Sheffield, Sheffield S3 7RH, UK

ABSTRACT. Beyond ~13.9 cal kBP, the IntCal20 radiocarbon (^{14}C) calibration curve is based upon combining data across a range of different archives including corals and planktic foraminifera. In order to reliably incorporate such marine data into an atmospheric curve, we need to resolve these records into their constituent atmospheric signal and marine reservoir age. We present results of marine reservoir age simulations enabling this resolution, applying the LSG ocean general circulation model forced with various climatic background conditions and atmospheric radiocarbon changes according to the Hulu Cave speleothem record. Simulating the spatiotemporal evolution of reservoir ages between 54,000 and 10,700 cal BP, we find reservoir ages between 500 and 1400 yr in the low- and mid-latitudes, but also more than 3000 yr in the polar seas. Our results are broadly in agreement with available marine radiocarbon reconstructions, with the caveat that continental margins, marginal seas, or tropical lagoons are not properly resolved in our coarse-resolution model.

KEYWORDS: marine reservoir age, modeling.

INTRODUCTION

The spatiotemporal variability of marine radiocarbon (^{14}C) records is superimposed by a systematic isotopic depletion with respect to the atmosphere. This effect is frequently expressed as marine reservoir age (MRA) and has to be taken into account when ^{14}C calibration considers marine archives (Alves et al. 2018). Prebomb MRAs have ranged from ~400 yr in subtropical oceans to more than 1000 yr in polar seas (Key et al. 2004). Prior to the continuous tree-ring record, MRAs are poorly constrained and have to be inferred from ad-hoc assumptions or through modeling.

IntCal20 aims to reconstruct the atmospheric ^{14}C concentration at mid-latitudes in the Northern Hemisphere. From 0 to ~13.9 cal kBP, IntCal20 is constructed from dendrochronologically dated tree rings providing direct atmospheric observation. However, further back in time, the lack of available trees means that a variety of alternative archives are required including macro-fossils, speleothems, corals and planktic foraminifera. Each of these archives have their own specific characteristics. In particular, the use of data from marine environments (such as corals and foraminifera) is complicated by the MRA meaning such observations are offset, probably floating in space and time, from the atmospheric ^{14}C we wish to reconstruct. To reliably reconstruct atmospheric ^{14}C, we therefore need to be able to resolve such records into their constituent atmospheric and MRA components.

To provide such a resolution for IntCal20, we have taken the following approach. Firstly, we construct a preliminary estimate for atmospheric ^{14}C based solely upon the Hulu cave record (Southon et al. 2012; Cheng et al. 2018). This Hulu-Cave-based atmospheric ^{14}C reconstruction is then fed into an ocean general circulation model (Butzin et al. 2017) to provide temporal MRA estimates at all of our marine sites contributing to IntCal. These MRA estimates are then fed back into the construction of the main IntCal20 atmospheric curve allowing us to compile the MRA-adjusted marine records alongside the other archives, see Heaton et al. (2020 in this issue) for further details. Such an approach can be seen somewhat

---

*Corresponding author. Email: martin.butzin@awi.de.

analogously to the first step in an iterative backfitting procedure (or a single update of the MRA within a wider Markov Chain Monte Carlo method). While ideally one may wish to iterate this procedure several times to improve MRA estimation, we believe a single run will provide a reliable first-order approximation. Here, we give an overview of the applied simulation scenarios to create these MRA estimates given the Hulu-Cave-based curve and briefly discuss the results.

METHOD

We employ the Hamburg Large Scale Geostrophic (LSG) ocean general circulation model (Maier-Reimer et al. 1993) with a horizontal resolution of 3.5° and a vertical resolution of 22 unevenly spaced levels. The LSG model has been constantly improved by including a bottom boundary layer scheme (Lohmann 1998), a sophisticated numerical advection scheme (Schäfer-Neth and Paul 2001; Prange et al. 2003) and has demonstrated its skills in ^{14}C simulations (Butzin et al. 2005, 2012, 2017). In the current setup, the model can simulate the entire radiocarbon timescale (~60 kyr) within a few days of CPU time on state-of-the-art computer systems. The model is forced with monthly fields of recent and glacial wind stress, surface air temperature, and freshwater flux derived in previous climate simulations (Lohmann and Lorenz 2000; Prange et al. 2004). In the same way as in our precursor study (Butzin et al. 2017), we consider three climate forcing scenarios to assess the impact of past ocean-climate variability on marine ^{14}C records. To summarize, scenario PD employs present-day climate background conditions approximating the Holocene and interstadials. Glacial scenario GS aims at representing the Last Glacial Maximum (LGM), featuring a shallower Atlantic meridional overturning circulation (AMOC) weakened by about 30% compared to PD. A second glacial climate scenario (CS) mimics cold stadials with further AMOC weakening by about 60%. A thorough discussion of these scenarios can be found in Butzin et al. (2005).

Radiocarbon is simulated on-line as $F^{14}R_{\text{oce-atm}}$ (the ^{14}C enrichment of the ocean relative to the contemporaneous atmosphere, Soulet et al. 2016) following Toggweiler et al. (1989). That is, we do not consider ^{14}C and ^{12}C separately but directly simulate their fractionation-corrected ratio. This approach neglects biological effects which are one order of magnitude smaller than the effects of ocean circulation and radioactive decay on $F^{14}R_{\text{oce-atm}}$ (Fiadeiro 1982). Oceanic uptake of ^{14}C is calculated according to Sweeney et al. (2007), using atmospheric CO_2 concentrations as compiled in the spline of Köhler et al. (2017) and prescribed time-invariant concentrations of dissolved inorganic carbon in surface water as simulated by Hesse et al. (2011). As described in the introduction, atmospheric ^{14}C forcing was based solely upon the Hulu Cave speleothem record with a Dead Carbon Fraction (DCF) of about (450 ± 70) ^{14}C yr (Southon et al. 2012; Cheng et al. 2018). To create this Hulu-Cave-based atmospheric curve, the same Bayesian spline errors-in-variables statistical methodology was used as in construction of the final IntCal20 curve (Heaton et al. 2020 in this issue). Within each individual speleothem, the DCF was considered constant but taking potentially different levels for each speleothem in the cave. Priors for the DCF of each speleothem were taken from the relevant papers of Southon et al. (2012) and Cheng et al. (2018). The spline-based Markov Chain Monte Carlo (MCMC) was run for 250,000 iterations (with the first half being discarded as burn-in) to obtain a posterior mean estimate for the Hulu-based ^{14}C atmospheric reconstruction along with upper and lower 95% credible (2-sigma) pointwise intervals (see Figure 1).

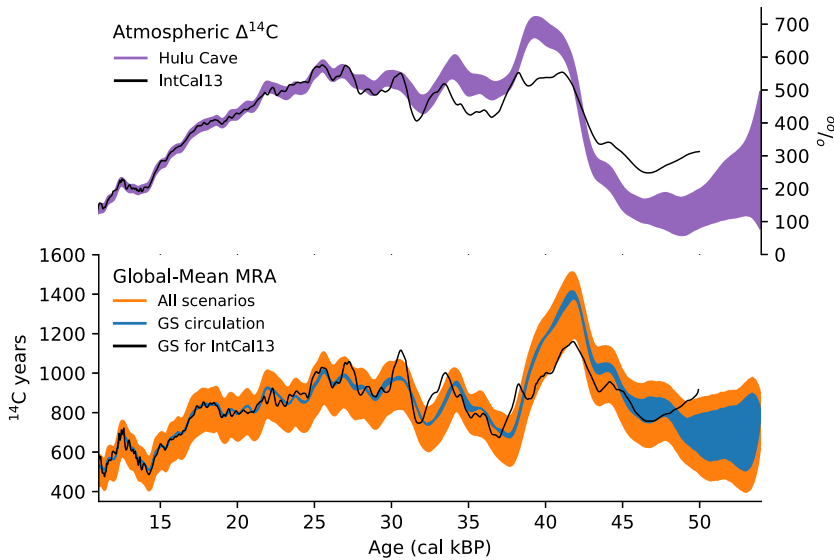Figure 1   (Top) Atmospheric $\Delta^{14}C$ from the Hulu Cave record (Southon et al. 2012; Cheng et al. 2018) used as transient forcing in our simulations. Plotted band spans the uncertainty range (mean values ±2 σ). (Bottom) Simulated global mean marine reservoir ages (MRA) in the upper 50 m, plotted are global averages excluding regions poleward of 50° latitude. Upper and lower bounds of all results are plotted in orange. Scenario GS is plotted in blue. The black lines show previous model results for scenario GS (Butzin et al. 2017) forced with atmospheric $\Delta^{14}C$ according to IntCal13 (Reimer et al. 2013). (Please see electronic version for color figures.)

We combine all three ocean climates (PD, GS, and CS) and all three ^{14}C forcing scenarios (posterior mean, upper and lower 95% credible intervals) to create nine numerical experiments. Each experiment is spun up over 20,000 yr with fixed atmospheric values of ^{14}C and CO_2 at 54 cal kBP ($\Delta^{14}C_{atm}$ = 73–504‰ and pCO_2 = 219 μatm), before the model is run transiently forward in time until 10.7 cal kBP forced by time-variable ^{14}C and pCO_2 values. Marine reservoir ages are calculated afterwards in ^{14}C-yr as MRA = –8033 × ln ($F^{14}R_{oce-atm}$), based on simulation results for the upper 50 m of the ocean corresponding to the typical habitat depth of corals and foraminifera analyzed in IntCal20. The impact of different ocean surface depth ranges on MRA has been analyzed in Butzin et al. (2017) and is not investigated any further here.

RESULTS AND DISCUSSION

Figure 1 shows the simulated history of global-mean MRAs. The envelope spans all MRA simulations and may be interpreted as total uncertainty range. A closer look at the MRA uncertainty of any specific ocean climate scenario, e.g. scenario GS, indicates that the contribution of the atmospheric ^{14}C forcing uncertainty is small between 10.7 and ~44 cal kBP. That is, the uncertainty of simulated MRAs is largely due to the difference in the three climate scenarios, with the upper or lower bound corresponding to scenario CS or PD, respectively.

In the following discussion we focus on scenario GS, as (most) MRA estimates in IntCal20 are based on this scenario, which also corresponds to the ensemble median of simulated MRAs when forced with the mean atmospheric ^{14}C record. Disregarding high-latitude regions
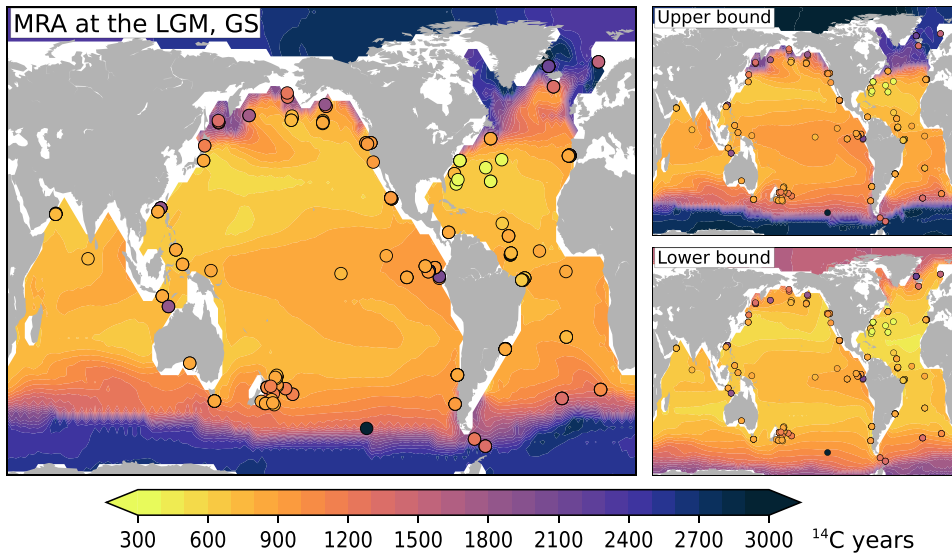
Figure 2   Geographic distribution of simulated marine reservoir ages (MRAs) in the upper 50 m at the Last Glacial Maximum (time average over 19–23 cal kBP). Left: Results for scenario GS forced with the mean atmospheric $\Delta^{14}C$ record; right: upper and lower bounds of all simulation results involving scenarios CS (top) and PD (bottom). Filled circles are foraminifera-based MRAs compiled by Skinner et al. (2017).

where sea ice inhibits oceanic $^{14}CO_2$ uptake, we find global mean MRA variations between 500 and 1400 ^{14}C yr. The lowest reservoir ages are simulated during the last deglaciation with two minima around 11 and 14 cal kBP caused by the combination of small atmospheric ^{14}C values and rising concentrations of atmospheric CO_2, the latter allowing a higher oceanic $^{14}CO_2$ uptake. At the LGM (19–23 cal kBP) the global mean MRA was about 800 ^{14}C yr. Prior to the LGM our simulations show variations in global mean MRA of several hundreds of years with positive anomalies associated with the Mono Lake (~34 cal kBP, Lund et al. 2017) and Laschamps (~42 cal kBP, Lascu et al. 2016) geomagnetic excursions. In our precursor study (considering scenario GS and atmospheric ^{14}C according to IntCal13, black line in Figure 1) the amplitude of these variations was slightly larger between 27 cal kBP and 34 cal kBP, but more than 200 ^{14}C yr smaller around the Laschamps excursion. This is due to the revised atmospheric ^{14}C forcing during this period. Note that the global mean MRA peak at 42 cal kBP precedes the atmospheric ^{14}C maximum by about 3000 cal yr. Instead, the global mean MRA peak coincides with an inflection point of the atmospheric ^{14}C forcing curve after which the slowly adjusting ocean is able to catch up with the ^{14}C excursion in the atmosphere.

Since the climate scenarios applied here are identical to those used in our previous work, we also find—as expected—similar results: the youngest surface waters are always found in the subtropical oceans and the oldest surface waters in the polar seas, where ice cover can boost MRAs to more than 3000 ^{14}C yr. During the LGM the general spatial pattern of the MRA is in line with the few data-based MRA reconstructions (Skinner et al. 2017) available for this time slice (Figure 2).

Here, the lowest MRAs are simulated for the subtropical Northeast Pacific where ^{14}C paleorecords are particularly scarce. However, in no scenario we arrive at such low MRAs close to preindustrial values as contained in the reconstruction for the subtropical Northwest Atlantic (Skinner et al. 2017). To assess potential model biases not only for a single date but
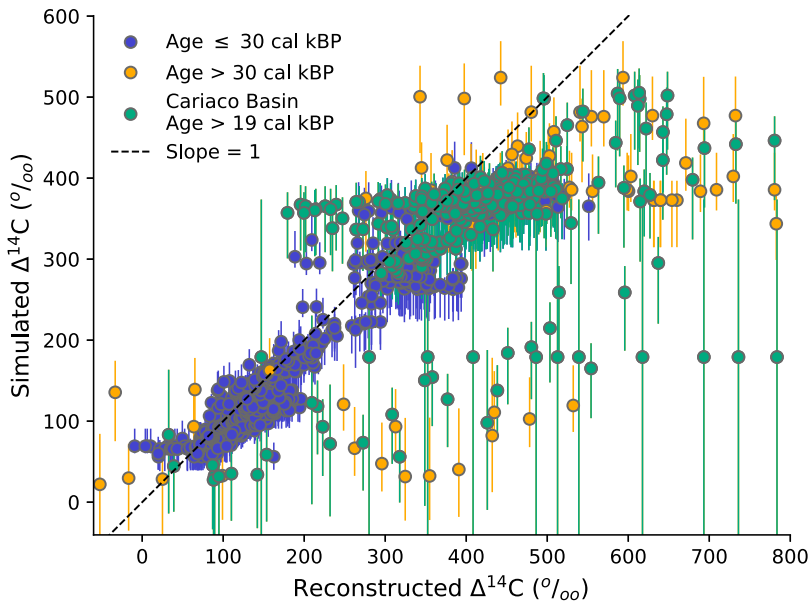
Figure 3 Comparison of simulated and reconstructed marine Δ^{14}C for locations which contain records contributing to IntCal20 (Bard et al. 1990, 1998, 2004a, 2004b, 2013; Burr et al. 1998, 2004; Hughen et al. 2000, 2004, 2006; Cutler et al. 2004; Fairbanks et al. 2005; Durand et al. 2013; Heaton et al. 2013). Simulation results are for ocean climate scenario GS forced with the mean atmospheric Δ^{14}C record where error bars indicate the combined uncertainty of atmospheric Δ^{14}C and scenarios CS and PD. Four data points are not shown (two data points with reconstructed Δ^{14}C < –150‰ and simulated Δ^{14}C ~20‰, plus two data points with reconstructed Δ^{14}C > 1500‰ and simulated Δ^{14}C ~200‰).

for the entire simulation period, we compare reconstructed marine Δ^{14}C records contributing to IntCal20 with marine Δ^{14}C simulated at nearby grid cells, keeping in mind that none of these sites is representative for open-ocean conditions for which the LSG model has been designed. This is shown as scatterplot in Figure 3, in which unbiased model results and reconstructions should align along a straight line with slope = 1 and intercept = 0. Our simulations frequently underestimate marine Δ^{14}C prior to ~30 cal kBP where the uncertainties in the reconstructions are large. Simulated Δ^{14}C is also low in the Cariaco Basin prior to ~19 cal kBP.

The underestimate of simulated Δ^{14}C suggests that the MRAs derived for these data points may be too high or that much of the coral data older than 30 ka BP has undergone diagenesis. The Cariaco Basin Δ^{14}C data could be reconciled with our simulations by assuming unrealistically large variations in the dead carbon fraction of the Hulu Cave ^{14}C record. Instead, IntCal20 has used another approach (Bayesian adaptive learning, see Heaton et al. 2020 in this issue) to estimate past MRAs in this specific marine environment. The LSG model resolution of ~380 km in the region of the Cariaco Basin is too coarse to capture its small depression (160 km long, 60 km wide) on the continental shelf off Venezuela, which was decoupled from the open Caribbean during the last glacial sea level lowstand (Peterson et al. 1991). First MRA simulations utilizing a global ocean general circulation model with enhanced resolution down to ~20 km in marginal seas (FESOM2 developed by Danilov et al. 2017) show promising improvements for the Cariaco region but long-term simulations, which would be necessary for a potential application of FESOM2 within this calibration effort here, are not yet available.

ACKNOWLEDGMENTS

REFERENCES

Alves EQ, Macario K, Ascough P, Bronk Ramsey C. 2018. The worldwide marine radiocarbon reservoir effect: Definitions, mechanisms, and prospects. Reviews of Geophysics 56:278–305. doi: 10.1002/2017RG000588.

Bard E, Arnold M, Hamelin B, Tisnerat-Laborde N, Cabioch G. 1998. Radiocarbon calibration by means of mass spectrometric ^{230}Th/^{234}U and ^{14}C ages of corals. An updated data base including samples from Barbados, Mururoa and Tahiti. Radiocarbon 40:1085–1092.

Bard E, Hamelin B, Fairbanks RG, Zindler A. 1990. Calibration of the ^{14}C timescale over the past 30,000 years using mass spectrometric U-Th ages from Barbados corals. Nature 345(6274):405–410. doi: 10.1038/345405a0.

Bard E, Ménot G, Rostek F, Licari L, Böning P, Edwards RL, Cheng H, Wang Y, Heaton TJ. 2013. Radiocarbon calibration/comparison records based on marine sediments from the Pakistan and Iberian Margins. Radiocarbon 55:1999–2019.

Bard E, Rostek F, Ménot-Combes G. 2004a. Radiocarbon calibration beyond 20,000 ^{14}C yr B.P. by means of planktonic foraminifera of the Iberian Margin. Quaternary Research 61:204–214. doi: 10.1016/j.yqres.2003.11.006.

Bard E, Ménot-Combes G, Rostek F. 2004b. Present status of radiocarbon calibration and comparison records based on Polynesian corals and Iberian Margin sediments. Radiocarbon 46:1189–1202.

Burr GS, Beck JW, Taylor FW, Recy J, Edwards RL, Cabioch G, Correge T, Donahue DJ, O'Malley JM. 1998. A high-resolution radiocarbon calibration between 11,700 and 12,400 calendar years BP derived from ^{230}Th ages of corals from Espiritu Santo Island, Vanuatu. Radiocarbon 40:1093–1105.

Burr GS, Galang C, Taylor FW, Gallup C, Edwards RL, Cutler K, Quirk B. 2004. Radiocarbon Results from a 13-Kyr BP coral from the Huon Peninsula, Papua New Guinea. Radiocarbon 46:1211–1224.

Butzin M, Köhler P, Lohmann G. 2017. Marine radiocarbon reservoir age simulations for the past 50,000 years. Geophysical Research Letters 44(16):8473–8480. doi: 10.1002/2017GL074688.

Butzin M, Prange M, Lohmann G. 2005. Radiocarbon simulations for the glacial ocean: The effects of wind stress, Southern Ocean sea ice and Heinrich events. Earth and Planetary Science Letters 235(1–2):45–61. doi: 10.1016/j.epsl.2005.03.003.

Butzin M, Prange M, Lohmann G. 2012. Readjustment of glacial radiocarbon chronologies by self-consistent three-dimensional ocean circulation modeling. Earth and Planetary Science Letters 317–318:177–184. doi: 10.1016/j.epsl.2011.11.046.

Cheng H, Edwards RL, Southon J, Matsumoto K, Feinberg JM, Sinha A, Zhou W, Li H, Li X, Xu Y, et al. 2018. Atmospheric ^{14}C/^{12}C changes during the last glacial period from Hulu Cave. Science 362(6420):1293–1297. doi: 10.1126/science.aau0747.

Cutler KB, Gray SC, Burr GS, Edwards RL, Taylor FW, Cabioch, G, Beck JW, Cheng H, Moore, J. 2004. Radiocarbon calibration to 50 kyr BP with paired ^{14}C and ^{230}Th dating of corals from Vanuatu and Papua New Guinea. Radiocarbon 46:1127–1160.

Danilov S, Sidorenko D, Wang Q, Jung T. 2017. The Finite-volumE Sea ice–Ocean Model (FESOM2). Geoscientific Model Development 10(2):765–789. doi: 10.5194/gmd-10-765-2017.

Durand N, Deschamps P, Bard E, Hamelin B, Camoin G, Thomas AL, Henderson GM, Yokoyama Y, Matsuzaki H. 2013. Comparison of ^{14}C and U-Th ages in corals from IODP #310 cores offshore Tahiti. Radiocarbon. 55:1947–1974. doi: 10.2458/azu_js_rc.v55i2.16134.

Fairbanks RG, Mortlock RA, Chiu T-C, Cao L, Kaplan A, Guilderson TP, Fairbanks TW, Bloom AL, Grootes PM, Nadeau M-J. 2005. Radiocarbon calibration curve spanning 0 to 50,000 years BP based on paired ^{230}Th/^{234}U/^{238}U and ^{14}C dates on pristine corals. Quaternary Science Reviews 24(16–17):1781–1796. doi: 10.1016/j.quascirev.2005.04.007.

Fiadeiro ME. 1982. Three-dimensional modeling of tracers in the deep Pacific Ocean, II. Radiocarbon and the circulation. Journal of Marine Research 40:537–550.

Heaton TJ, Bard E, Hughen KA. 2013. Elastic tie-pointing—transferring chronologies between records via a Gaussian Process. Radiocarbon 55(4):1975–1997. doi: 10.2458/azu_js_rc.55.17777.

Heaton TJ, Blaauw M, Blackwell PG, Bronk Ramsey C, Reimer PJ, Scott ME. 2020. The IntCal20 approach to radiocarbon calibration curve construction: A new methodology using Bayesian splines and errors-in-variables. Radiocarbon 62. This issue.

Hesse T, Butzin M, Bickert T, Lohmann G. 2011. A model-data comparison of $\delta^{13}C$ in the glacial Atlantic Ocean. Paleoceanography 26(3). doi: 10.1029/2010PA002085.

Hughen K, Southon J, Lehman S, Bertrand C, Turnbull J. 2006. Marine-derived ^{14}C calibration and activity record for the past 50,000 years updated from the Cariaco Basin. Quaternary Science Reviews 25(23–24):3216–3227. doi: 10.1016/j.quascirev.2006.03.014.

Hughen KA, Southon JR, Bertrand CJH, Frantz B, Zermeño P. 2004. Cariaco Basin calibration update: Revisions to calendar and ^{14}C chronologies for Core Pl07-58Pc. Radiocarbon 46(3):1161–1187. doi: 10.1017/S0033822200033075.

Hughen KA, Southon JR, Lehman SJ, Overpeck JT. 2000. Synchronous radiocarbon and climate shifts during the last deglaciation. Science 290(5498): 1951. doi: 10.1126/science.290.5498.1951.

Key RM, Kozyr A, Sabine CL, Lee K, Wanninkhof R, Bullister JL, Feely RA, Millero FJ, Mordy C, Peng T-H. 2004. A global ocean carbon climatology: Results from Global Data Analysis Project (GLODAP). Global Biogeochem Cycles 18(4):GB4031. doi: 10.1029/2004GB002247.

Köhler P, Nehrbass-Ahles C, Schmitt J, Stocker TF, Fischer H. 2017. A 156 kyr smoothed history of the atmospheric greenhouse gases CO_2, CH_4, and N_2O and their radiative forcing. Earth System Science Data 9(1):363–387. doi: https://doi.org/10.5194/essd-9-363-2017.

Lascu I, Feinberg JM, Dorale JA, Cheng H, Edwards RL. 2016. Age of the Laschamp excursion determined by U-Th dating of a speleothem geomagnetic record from North America. Geology 44(2):139–142. doi: 10.1130/G37490.1.

Lohmann G. 1998. The influence of a near-bottom transport parameterization on the sensitivity of the thermohaline circulation. J. Phys. Oceanogr. 28(10):2095–2103. doi: 10.1175/1520-0485(1998)028<2095:TIOANB>2.0.CO;2.

Lohmann G, Lorenz S. 2000. On the hydrological cycle under paleoclimatic conditions as derived from AGCM simulations. J. Geophys. Res. 105 (D13):17417–17436. doi: 10.1029/2000JD900189.

Lund S, Benson L, Negrini R, Liddicoat J, Mensing S. 2017. A full-vector paleomagnetic secular variation record (PSV) from Pyramid Lake (Nevada) from 47–17 ka: Evidence for the successive Mono Lake and Laschamp Excursions. Earth and Planetary Science Letters 458:120–129. doi: 10.1016/j.epsl.2016.09.036.

Maier-Reimer E, Mikolajewicz U, Hasselmann K. 1993. Mean circulation of the Hamburg LSG OGCM and its sensitivity to the thermohaline surface forcing. J. Phys. Oceanogr. 23(4):731–757. doi: 10.1175/1520-0485(1993)023<0731:MCOTHL>2.0.CO;2.

Peterson LC, Overpeck JT, Kipp NG, Imbrie J. 1991. A high-resolution Late Quaternary upwelling record from the anoxic Cariaco Basin, Venezuela. Paleoceanography 6(1):99–119. doi: 10.1029/90PA02497.

Prange M, Lohmann G, Paul A. 2003. Influence of vertical mixing on the thermohaline hysteresis: Analyses of an OGCM. J. Phys. Oceanogr. 33(8): 1707–1721. doi: 10.1175/2389.1.

Prange M, Lohmann G, Romanova V, Butzin M. 2004. Modelling tempo-spatial signatures of Heinrich Events: influence of the climatic background state. Quaternary Science Reviews 23(5–6): 521–527. doi: 10.1016/j.quascirev.2003.11.004.

Reimer PJ, Bard E, Bayliss A, Beck JW, Blackwell PG, Bronk Ramsey C, Buck CE, Cheng H, Edwards RL, Friedrich M, Grootes PM, Guilderson TP, Haflidason H, Hajdas I, Hatté C, Heaton TJ, Hoffman DL, Hogg AG, Hughen KA, Kaiser KF, Kromer B, Manning SW, Niu M, Reimer RW, Richards DA, Scott EM, Southon JR, Staff RA, Turney CSM, van der Plicht J. 2013. IntCal13 and Marine13 radiocarbon age calibration curves 0–50,000 years cal BP. Radiocarbon 55(4): 1869–1887. doi: 10.2458/azu_js_rc.55.16947.

Schäfer-Neth C, Paul A. 2001. Circulation of the glacial Atlantic: a synthesis of global and regional modeling. In: Schäfer P, Ritzrau W, Schlüter M, Thiede J, editors. The Northern North Atlantic: A changing environment. Berlin: Springer. p. 446–462.

Skinner LC, Primeau F, Freeman E, Fuente M de la, Goodwin PA, Gottschalk J, Huang E, McCave IN, Noble TL, Scrivner AE. 2017. Radiocarbon constraints on the glacial ocean circulation and its impact on atmospheric CO_2. Nature Communications 8:16010. doi: 10.1038/ncomms16010.

Soulet G, Skinner LC, Beaupré SR, Galy V. 2016. A note on reporting of reservoir ^{14}C disequilibria and age offsets. Radiocarbon doi: 10.1017/RDC.2015.22.

Southon J, Noronha AL, Cheng H, Edwards RL, Wang YJ. 2012. A high-resolution record of atmospheric C-14 based on Hulu Cave speleothem H82. Quaternary Science Reviews 33:32–41. doi: 10.1016/j.quascirev.2011.11.022.

Sweeney C, Gloor E, Jacobson AR, Key RM, McKinley G, Sarmiento JL, Wanninkhof R. 2007. Constraining global air-sea gas exchange for CO_2 with recent bomb ^{14}C measurements. Global Biogeochem Cycles. 21(2):GB2015. doi: 10.1029/2006GB002784.

Toggweiler JR, Dixon K, Bryan K. 1989. Simulations of radiocarbon in a coarse-resolution world ocean model: 1. Steady state prebomb distributions. J. Geophys. Res. 94(C6):8217–8242. doi: 10.1029/JC094iC06p08217.